PCCP

Investigation of a Bacteriochlorin-Containing Pentad Array for Panchromatic Light-Harvesting and Charge Separation

Journal:	*Physical Chemistry Chemical Physics*
Manuscript ID	CP-ART-11-2022-005400.R1
Article Type:	Paper
Date Submitted by the Author:	15-Dec-2022
Complete List of Authors:	Jing, Haoyu; North Carolina State University, Chemistry Magdaong, Nikki Cecil; Washington University, Chemistry Diers, James; University of California Riverside, Chemistry Kirmaier, Christine; Washington University, Chemistry Bocian, David; University of California Riverside, Department of Chemistry Holten, Dewey; Washington University, Department of Chemistry Lindsey, Jonathan; North Carolina State University, Department of Chemistry

Investigation of a Bacteriochlorin-Containing Pentad Array for Panchromatic Light-Harvesting and Charge Separation

Haoyu Jing,[1] Nikki Cecil M. Magdaong,[2] James R. Diers,[3]

Christine Kirmaier,[2] David F. Bocian,[3] Dewey Holten,[2] and Jonathan S. Lindsey[1]

[1] Department of Chemistry
North Carolina State University
Raleigh, North Carolina 27695-8204
E-mail: jlindsey@ncsu.edu

[2] Department of Chemistry
Washington University
St. Louis, Missouri 63130-4889
E-mail: holten@wustl.edu

[3] Department of Chemistry
University of California
Riverside, California 92521-0403
E-mail: david.bocian@ucr.edu

Abstract

A new pentad array designed to exhibit panchromatic absorption and charge separation has been synthesized and characterized. The array is comprised of a triad panchromatic absorber (a bis(perylene-monoimide)-porphyrin) to which are appended an electron acceptor (perylene-diimide) and an electron donor / hole acceptor (bacteriochlorin) in a crossbar arrangement. The motivation for incorporation of the bacteriochlorin versus a free-base or zinc chlorin utilized in prior constructs was to facilitate hole transfer to this terminal unit and thereby achieve a higher yield of charge separation across the array. The intense $S_0 \rightarrow S_1$ (Q_y) band of the bacteriochlorin also enhances absorption in the near-infrared spectral region. Due to synthetic constraints, a phenylethyne linker was used to join the bacteriochlorin to the core porphyrin of the panchromatic triad rather than the diphenylethyne linker employed for the prior chlorin-containing pentads.

Static and time-resolved photophysical studies reveal enhanced excited-state quenching for the pentad in benzonitrile and dimethyl sulfoxide compared to the prior chlorin-containing analogues. Success was only partial, however, as a long-lived charge separated state was not observed despite the improved energetics for the final ground-state hole/electron-shift reaction. The apparent reason is more facile competing charge-recombination due to the shorter bacteriochlorin–porphyrin linker that increases electronic coupling for this process. The studies highlight design criteria for balancing panchromatic absorption and long-lived charge separation in molecular architectures for solar-energy conversion.

Introduction

From its earliest beginnings, an aspirational goal of artificial photosynthesis has been to create model systems that mimic all of the natural machinery for conversion of an incident photon to stored energy.[1-9] Such machinery includes a photosynthetic unit (collection of pigments that harvest light for downstream use),[10] reaction center, and accompanying catalysts for reduction of carbon dioxide and oxidation of an electron donor (e.g., water, in plants and cyanobacteria). A general objective of such work has been to create architectures wherein fundamental processes of energy transfer, electron transfer, and hole transfer can be studied in systems more manageable than the native photosynthetic systems. The challenge of organizing pigments in abiotic systems has prompted the design and synthesis of diverse molecular arrays.[8,11-58]

In studies in artificial photosynthesis aimed at probing light-driven charge separation, a common motif is a triad in which light absorption by a central chromophore such as a porphyrin initiates electron transfer to a flanking acceptor moiety followed by ground-state hole/electron migration to the unit on the opposite leg. Recently, we added a new dimension to such studies by constructing pentads wherein the central chromophore is replaced with a (bis)perylene-porphyrin triad that exhibits panchromatic absorption spanning the blue to red spectral regions, thereby

functioning as an antenna.[59,60] Two such pentads denoted **C-T-PDI** and **ZnC-T-PDI** are shown in Chart 1. The panchromatic PMI-P-PMI triad unit (T) is composed of a porphyrin coupled via direct ethyne linkers to two perylene-monoimides. A free base or zinc chlorin hole acceptor (or electron donor) and a perylene-diimide (PDI) electron acceptor were installed at the two other *meso*-positions of the central porphyrin, creating an overall crossbar architecture. In addition to being charge donors/acceptors, the chlorin and PDI units provide complementary absorption to the panchromatic triad that increases light-harvesting capacity.

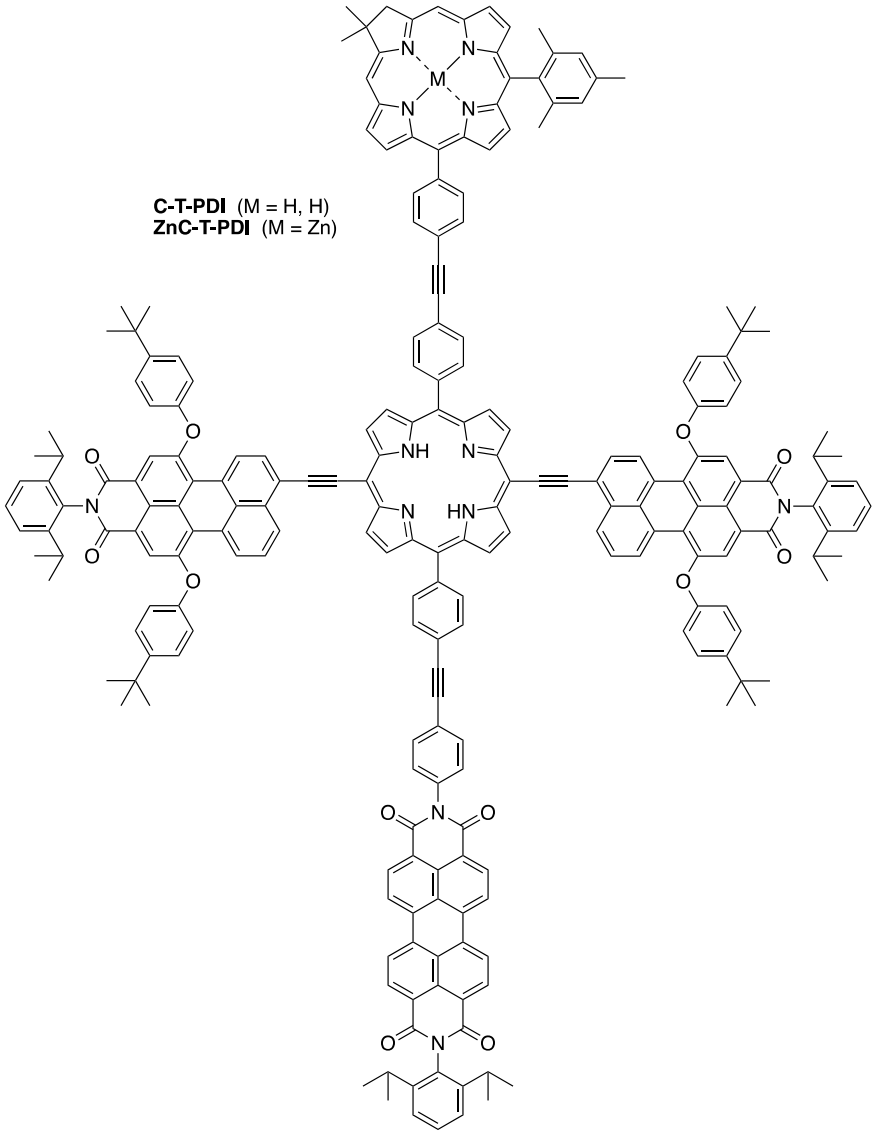

Chart 1. *meso*-Linked chlorin-porphyrin pentads synthesized previously.[59,60]

Static optical studies and ultrafast transient absorption (TA) measurements showed that excited-state electron transfer does not occur to a measurable extent for **C-T-PDI** in toluene or benzonitrile (PhCN). Excited-state quenching is observed for this pentad in dimethyl sulfoxide (DMSO), but is followed by charge-recombination that resulted in no detectable formation of the full charge-separated state C^+-T-PDI^-.[60] A potential bottleneck considered for **C-T-PDI** was shifting the hole from the panchromatic triad T to the terminal chlorin. Thus, pentad **ZnC-T-PDI** (Chart 1) was prepared because zinc chlorins are known to be easier to oxidize than their free-base chlorin counterparts.[61] Like **C-T-PDI**, pentad **ZnC-T-PDI** exhibits no excited-state hole/electron transfer in toluene, but unlike **C-T-PDI**, does so in PhCN. Charge-separated state ZnC^+-T-PDI^- was observed albeit in low (~5%) yield. The charge-separated state has much higher (~30%) yield for **ZnC-T-PDI** in DMSO and exhibits a lifetime of ~1 μs.[60] Thus, making the chlorin easier to oxidize markedly improved long-lived charge separation.

These prior results led to the design, synthesis and characterization of pentad **BC-T-PDI** (Chart 2) described herein. The bacteriochlorin unit in **BC-T-PDI** is linked with the central porphyrin via a phenylethynyl linker rather than the diphenylethynyl linker in **C-T-PDI** and **ZnC-T-PDI** (Chart 1) due to synthetic constraints. In addition to being easier to oxidize, the bacteriochlorin in **BC-T-PDI** has a Q_y ($S_0 \rightarrow S_1$) band that is more intense and is shifted bathochromically compared to that for chlorins in **C-T-PDI** and **ZnC-T-PDI**, thereby enhancing red-region absorption. Herein, we report the synthesis of new pentad **BC-T-PDI** and bacteriochlorin benchmark **MeOBC-1**. The photophysical properties of the compounds in toluene, PhCN, and DMSO were studied by static and time-resolved optical spectroscopy. Molecular-orbital (MO) characteristics were derived from density functional theory (DFT) calculations. Excited-state properties are obtained from time-dependent DFT (TDDFT) calculations.

Collectively, the results provide insights into design principles for constructing molecular arrays that combine capabilities for panchromatic absorption and charge separation.

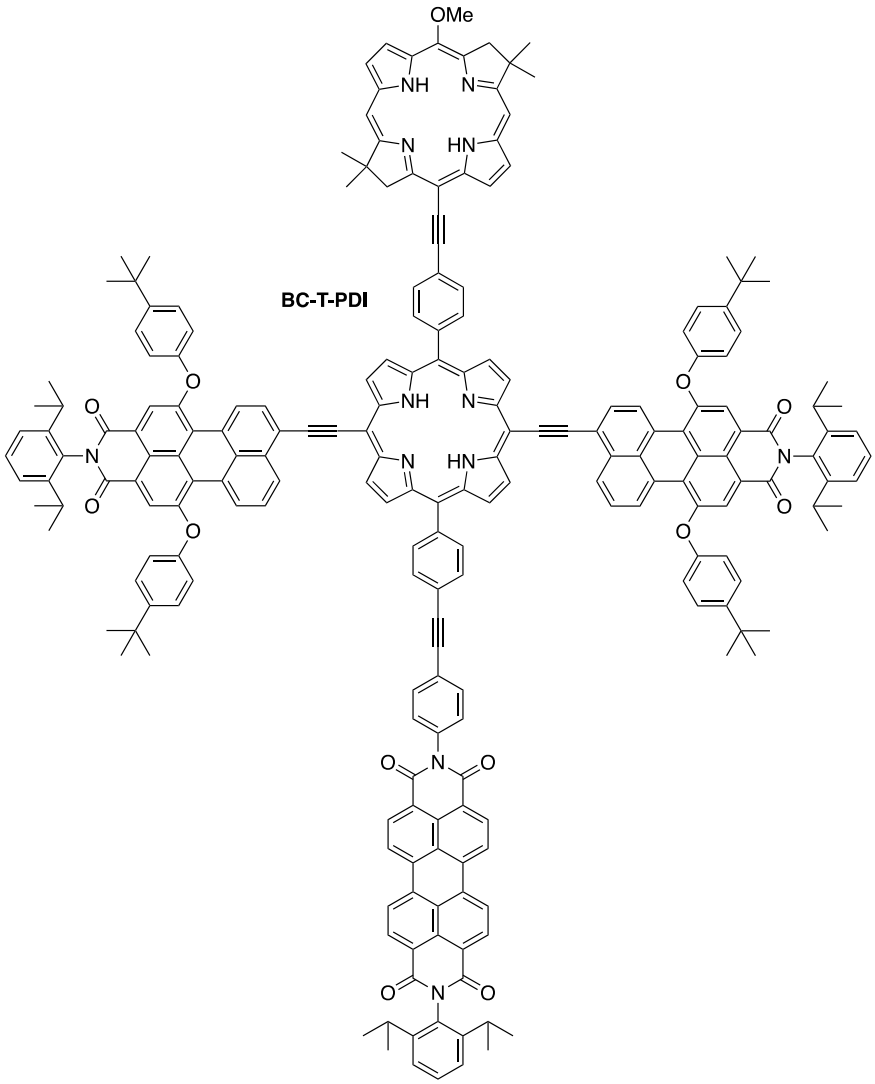

Chart 2. Bacteriochlorin pentad.

Results and Discussion

Synthesis. The synthesis of the bacteriochlorin pentad **BC-T-PDI** is shown in Scheme 1. The known[62] meso-brominated bacteriochlorin **MeOBC-Br** was coupled with known[59] tetrad **PDI-T-e** using a copper-free Sonogashira reaction[63,64] in toluene and triethylamine (TEA) to give **BC-T-PDI** in 65% yield. The ethynylation of meso-bromobacteriochlorins is well established.[65]

The purification of the bacteriochlorin-containing pentad follows the reported procedure for chlorin-containing analogues.[59,60] An outline is provided as follows. The crude mixture was purified by a two-step chromatography procedure. The crude product mixture was first concentrated and purified by preparative size-exclusion chromatography (SEC) using tetrahydrofuran (THF) as eluent to remove byproducts and impurities (e.g., bacteriochlorin, oligomers) and then silica was used to remove material derived from the SEC resin. The coupling reaction of phenylacetylene and **MeOBC-Br** under similar conditions[65] afforded the benchmark bacteriochlorin monomer **MeOBC-1** (Scheme 1).

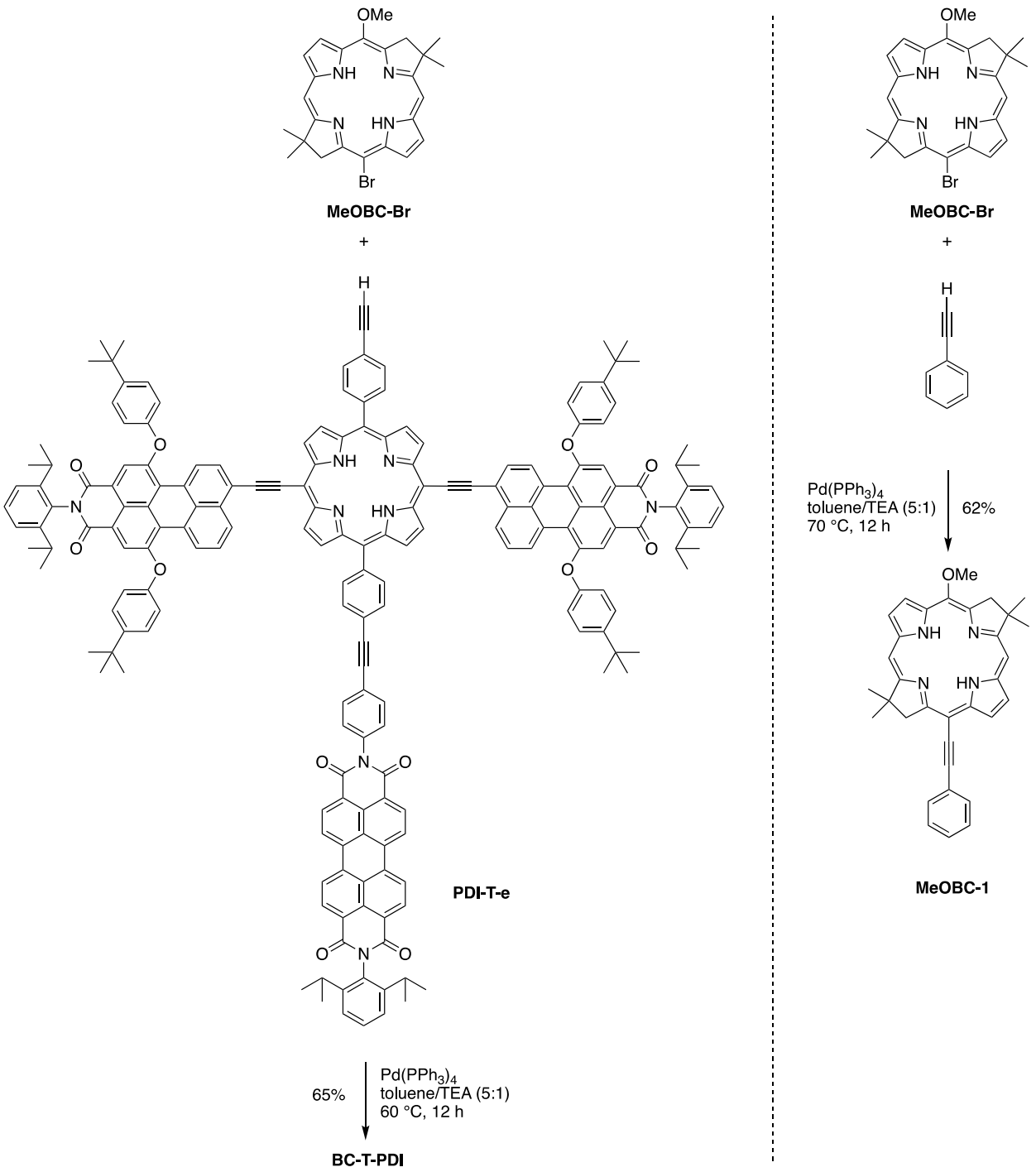

Scheme 1. Synthesis of pentad **BC-T-PDI** and a bacteriochlorin benchmark monomer.

Chemical characterization. The **BC-T-PDI** pentad array was homogeneous by analytical SEC,[66] and exhibited a retention time (~30.9 min) similar to that of **C-T-PDI** and of **ZnC-T-PDI** prepared previously[59,60] (Figure 1). The bacteriochlorin monomer (main peak after 30.9 min) and

other unidentified oligomers (peaks before 30.9 min) were removed using preparative SEC. The **BC-T-PDI** pentad was characterized by matrix-assisted laser-desorption ionization mass spectrometry (MALDI-MS) analysis using the matrix α-cyano-4-hydroxycinnamic acid. The pentad ($C_{215}H_{174}N_{12}O_{13}$, exact mass 3131.33 Da) gave a peak at *m/z* = 3132.728, consistent with $[M + H]^+$.

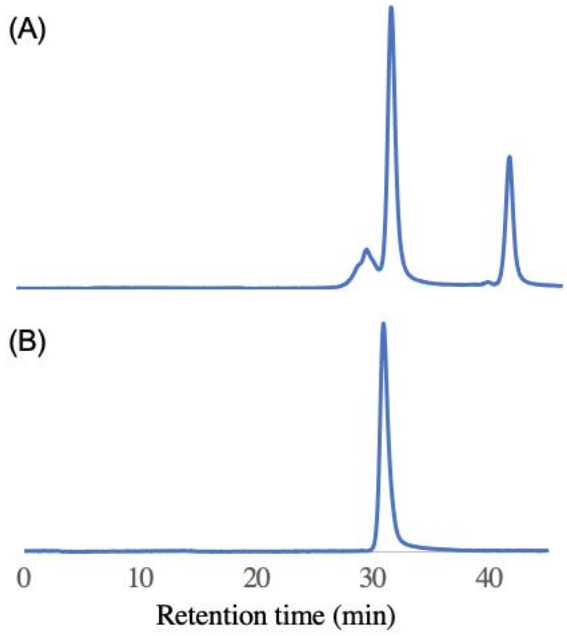

Figure 1. Analytical SEC trace (λ_{obs} = 640 nm) of (A) reaction mixture and (B) purified product (following preparative SEC).

Absorption spectra. Figure 2 compares the absorption spectrum of new pentad **BC-T-PDI** studied here with those for the analogous chlorin-based pentads **ZnC-T-PDI** and **C-T-PDI**. The incorporation of the bacteriochlorin in place of the zinc or free base chlorin increases the light-harvesting capacity of the architecture. This is seen from the enhanced absorption in the violet and red regions and an overall more uniform intensity distribution across the visible spectrum.

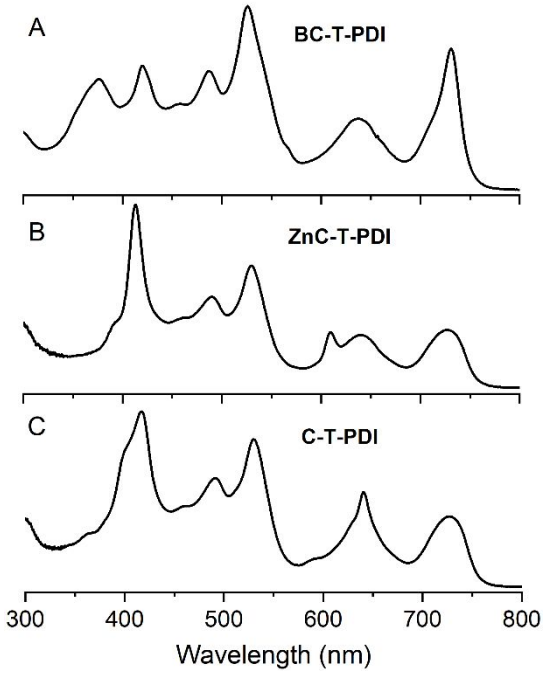

Figure 2. Absorption spectrum of pentads **BC-T-PDI** studied here (A) and previously investigated analogues **ZnC-T-PDI** (B) and **C-T-PDI** (C) in toluene.

The absorption spectrum of pentad **BC-T-PDI** (Figure 3A, red) is essentially the superposition (Figure 3A, black dashed) of the spectra (Figure 3B and C) of the tetrad **PDI-T-e** (violet) and bacteriochlorin monomer (blue) (**MeOBC-1**) that are joined by the phenylethyne linker (Scheme 1). While the analytical SEC indicated the pentad **BC-T-PDI** was homogeneous, the absorption spectrum indicated the presence of a small amount of an impurity. The origin of the impurity is unclear, yet its identification as a putative chlorin is suggested from the position of the absorption band (see asterisk in Figure 3, panel A). The presence of the impurity did not interfere with the studies reported herein (vide infra).

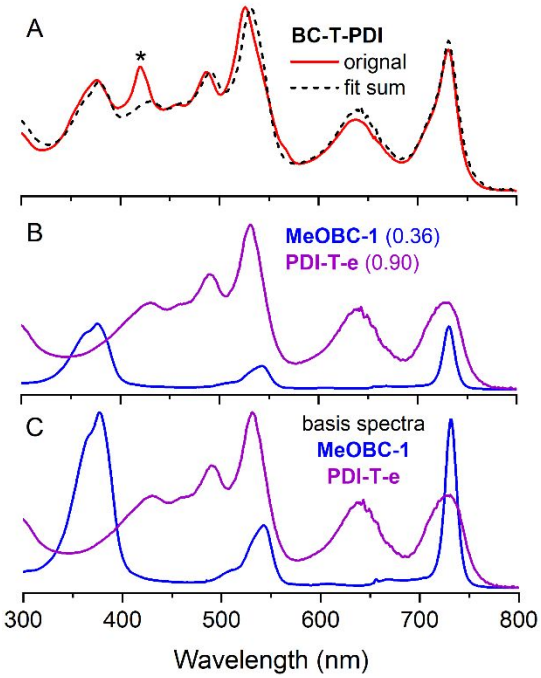

Figure 3. Absorption spectrum of pentad **BC-T-PDI** (red) and fit sum of spectra of the constituents (black dashed) in THF (A). The spectra of bacteriochlorin monomer **MeOBC-1** (blue) and tetrad **PDI-T-e** (violet) that were summed in panel A are shown in panel B along with the fractions (in parenthesis) of the normalized (at the largest peak) basis spectra shown in panel C. The asterisk for the feature at ~420 nm indicates a small putative chlorin impurity in **BC-T-PDI**.

Figure 4A shows the absorption spectrum of pentad **BC-T-PDI** in toluene, PhCN, and DMSO. The figure also shows the spectra of the benchmarks for the three functional subunits of the pentad in the same three solvents. These units are benchmark bacteriochlorin **MeOBC-1** (panel B), the PMI-P-PMI panchromatic triad **T-Ph** (panel C), and perylene-diimide **PDI-Ph** (panel D). The spectrum of the pentad is almost the same in toluene and PhCN but shows differences including increased breadth of the features in DMSO. These differences arise from the solvent dependence of the spectrum of the panchromatic triad (panels A and C). The structures of the two compounds for comparison purposes (**T-Ph**, **PDI-Ph**) are shown in Chart 3.

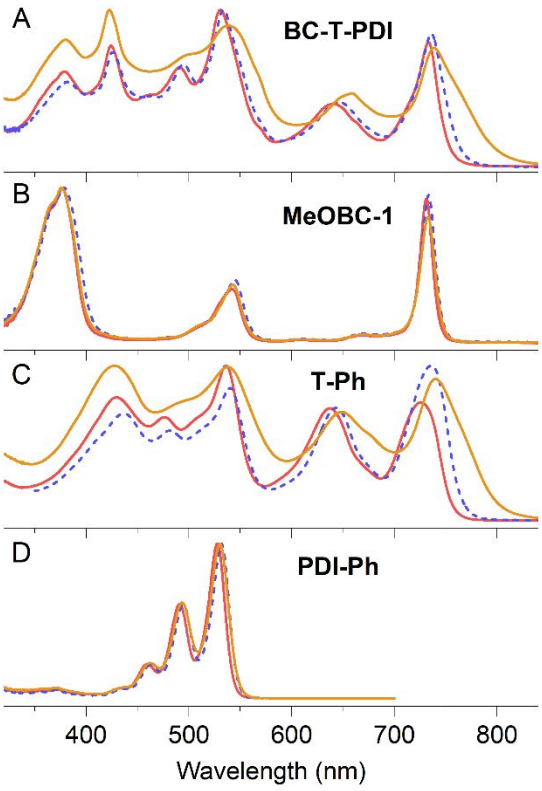

Figure 4. Absorption spectra of pentad **BC-T-PDI** (A), bacteriochlorin monomer **MeOBC-1** (B), benchmark triad **T-Ph** (C), and benchmark perylene-diimide **PDI-Ph** (D) in toluene (solid red), PhCN (dashed blue), and DMSO (solid gold).

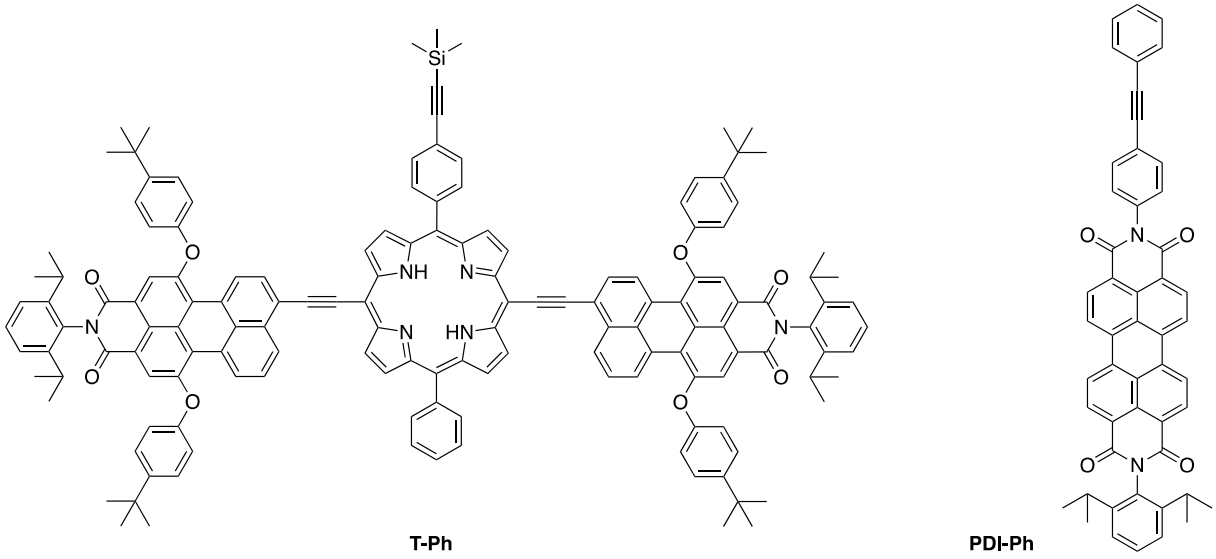

Chart 3. Benchmark compounds.

Fluorescence spectra. Fluorescence spectra of the bacteriochlorin-based pentad and bacteriochlorin monomer (in toluene, PhCN, and DMSO) are shown in Figures 5A and 5B, respectively. The spectra show the nominal $Q_y(0,0)$ main feature and the weaker $Q_y(0,1)$ satellite to longer wavelength. The Stokes shift between the $Q_y(0,0)$ absorption and fluorescence maxima is ≤1 nm (~20 cm^{-1}) for **MeOBC-1** in all three solvents. The shift is 3 nm (55 cm^{-1}) for **BC-T-PDI** in toluene, 7 nm (127 cm^{-1}) in DMSO, and 3 nm (236 cm^{-1}) in PhCN. In all solvents, the fluorescence spectrum for **BC-T-PDI**, like the $Q_y(0,0)$ absorption band, is broader than that for **MeOBC-1**.

The data in Figures 5A and 5B emphasize what is suggested by Figures 3 and 4 – that the energy of the S_1 excited state for **BC-T-PDI** lies very close in energy (<100 cm^{-1}) to that for **MeOBC-1**. [The TDDFT calculations described below for the pentad in toluene suggest that the S_1 state of the pentad resides on the bacteriochlorin.] Relevant here is Figure 5C, which shows the fluorescence spectrum and nominal $Q_y(0,0)$ absorption band of the previously studied panchromatic triad **T-Ph** in toluene, PhCN, and DMSO.[59,60] The near-infrared (NIR) absorption peak for **BC-T-PDI** is sharper than that for **T-Ph** (in all three solvents) and thus appears to have some bacteriochlorin character. The fluorescence spectra for **BC-T-PDI** in PhCN and DMSO are essentially the same as those for **T-Ph** in terms of shape and peak positions; the $Q_y(0,0)$ absorption band is also at approximately the same wavelength for the pentad and triad in both solvents. The fluorescence spectrum for **BC-T-PDI** in toluene has similar breadth to that of **T-Ph** (much broader than that for **MeOBC-1**) but is bathochromically shifted by 5 nm, similar to the 7-nm shift in the absorption maximum. These characteristics likely reflect interaction of the bacteriochlorin and panchromatic triad (T) components of pentad **BC-T-PDI**. The extent of the interactions likely stem from the effect of solvent on electronic properties (*e.g.,* $S_0 \rightarrow S_1$ absorption peak wavelength) of the panchromatic triad.

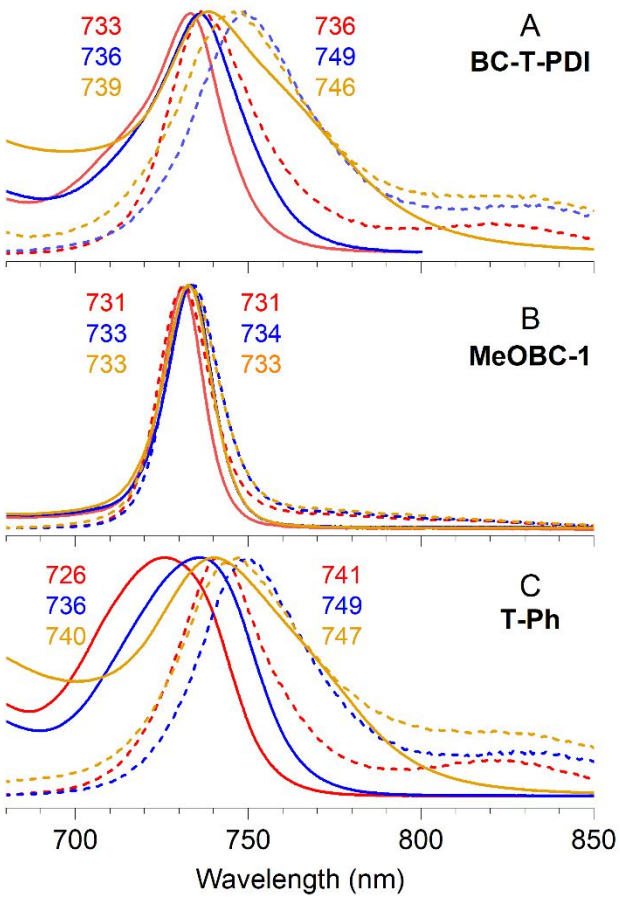

Figure 5. $S_0 \rightarrow S_1$ absorption (solid) and $S_1 \rightarrow S_0$ fluorescence (dashed) spectra of pentad **BC-T-PDI** (A), benchmark bacteriochlorin **MeOBC-1** (B), and previously studied[59,60] benchmark triad **T-Ph** (C) in toluene (red), PhCN (blue), and DMSO (gold).

Fluorescence quantum yields and singlet excited-state lifetimes. Values of the fluorescence quantum yield (Φ_f) and singlet excited-state lifetime (τ_S) for the pentad **BC-T-PDI** and bacteriochlorin **MeOBC-1** in toluene, PhCN, and DMSO are given in the top portion of Table 1. For comparison, the table also gives the data for the previously studied pentads that contain a zinc chlorin (**ZnC-T-PDI**) or free-base chlorin (**C-T-PDI**) as well as for benchmark panchromatic triad (**T-Ph**). The τ_S values were measured by time-correlated single photon counting (TCSPC) fluorescence decay measurements for lifetimes ≥0.5 ns. The measurements were confirmed by TA studies, which provided the sole source of τ_S determinations for **BC-T-PDI** (like **ZnC-T-PDI** studied previously) in PhCN (Table 1).

The combined Φ_f and τ_S values in Table 1 for pentad **BC-T-PDI** compared to those for triad **T-Ph** (and bacteriochlorin **MeOBC-1**) indicate the following: (1) There is little S_1 excited-state quenching for pentad **BC-T-PDI** in toluene, similar to what was found previously[60] for **ZnC-T-PDI** and **C-T-PDI**. (2) **BC-T-PDI** in PhCN exhibits substantial excited-state quenching, similar to what was found previously for **ZnC-T-PDI** in PhCN. (3) **BC-T-PDI** in DMSO exhibits even more extensive excited-state quenching, again similar to what was found previously for **ZnC-T-PDI** in DMSO. In both polar solvents, the quenching is more substantial for **BC-T-PDI** than **ZnC-T-PDI** due to the more rapid S_1 decay and lower fluorescence yield. The excited-state quenching must derive from hole/electron transfer. Such processes were probed via the TA studies described next.

Table 1. Photophysical properties of arrays.

Compound	SE#	Solvent	τ_s (ns)[a]	Φ_f[b]
Pentad				
BC-T-PDI	524	Toluene	2.4[c]	0.25
		PhCN	0.05[d]	0.044
		DMSO	0.01[d]	0.009
Monomer				
MeOBC-1	525	Toluene	5.2	0.25
		PhCN	5.2	0.22
		DMSO	4.8	0.22
Prior Arrays[e]				
ZnC-T-PDI	523	Toluene	2.0	0.34
		PhCN	0.17[f]	0.037
		DMSO	0.03[f]	0.007
C-T-PDI	522	Toluene	2.0	0.34
		PhCN	1.1	0.20
		DMSO	0.13[f]	0.013
T-Ph	451	Toluene	2.2	0.30
		PhCN	1.4	0.22
		DMSO	0.06[f]	0.08

[a]Measured by TCSPC unless noted otherwise. [b]Relative to *meso*-tetraphenylporphyrin in non-degassed toluene ($\Phi_f = 0.070$).[67] [c]A value of 2.5 ns is obtained from TCSPC and 2.3 ns from TA studies. [d]From TA studies here. [e]Data from ref. 60. [f]From TA studies in ref. 60.

Excited-state dynamics from transient-absorption studies. TA data are given in given in Figures S4–S11. These data comprise difference spectra and kinetic profiles for **BC-T-PDI** in toluene, PhCN, and DMSO using 420 nm and 745 nm excitation flashes. Representative TA data and kinetic profiles using λ_{ex} = 745 nm for the pentad in the three solvents spanning the spectral range 430–820 nm and the time window –2 ps to 7.5 ns are presented in Figure 6. Corresponding decay associated difference spectra (DADS) from global analysis of the spectral-temporal data sets obtained using λ_{ex} = 745 nm are given in Figure 7. The figure also gives the decay time constant for the kinetic component associated with each DADS. DADS summaries and in an expanded format using λ_{ex} = 745 nm and λ_{ex} = 420 nm are given in Figures S12–S16. The major spectral features and kinetic components for **BC-T-PDI** in the three solvents are the same using λ_{ex} = 745 nm and λ_{ex} = 420 nm. The differences are small sharp features due to dynamics associated with excitation of a small putative chlorin impurity using λ_{ex} = 420 nm (along with excitation of the triad T component of the pentad) that are not observed using λ_{ex} = 745 nm, as seen from comparison of spectra in the Supplemental Information. Here, the focus is on the data acquired using λ_{ex} = 745 nm.

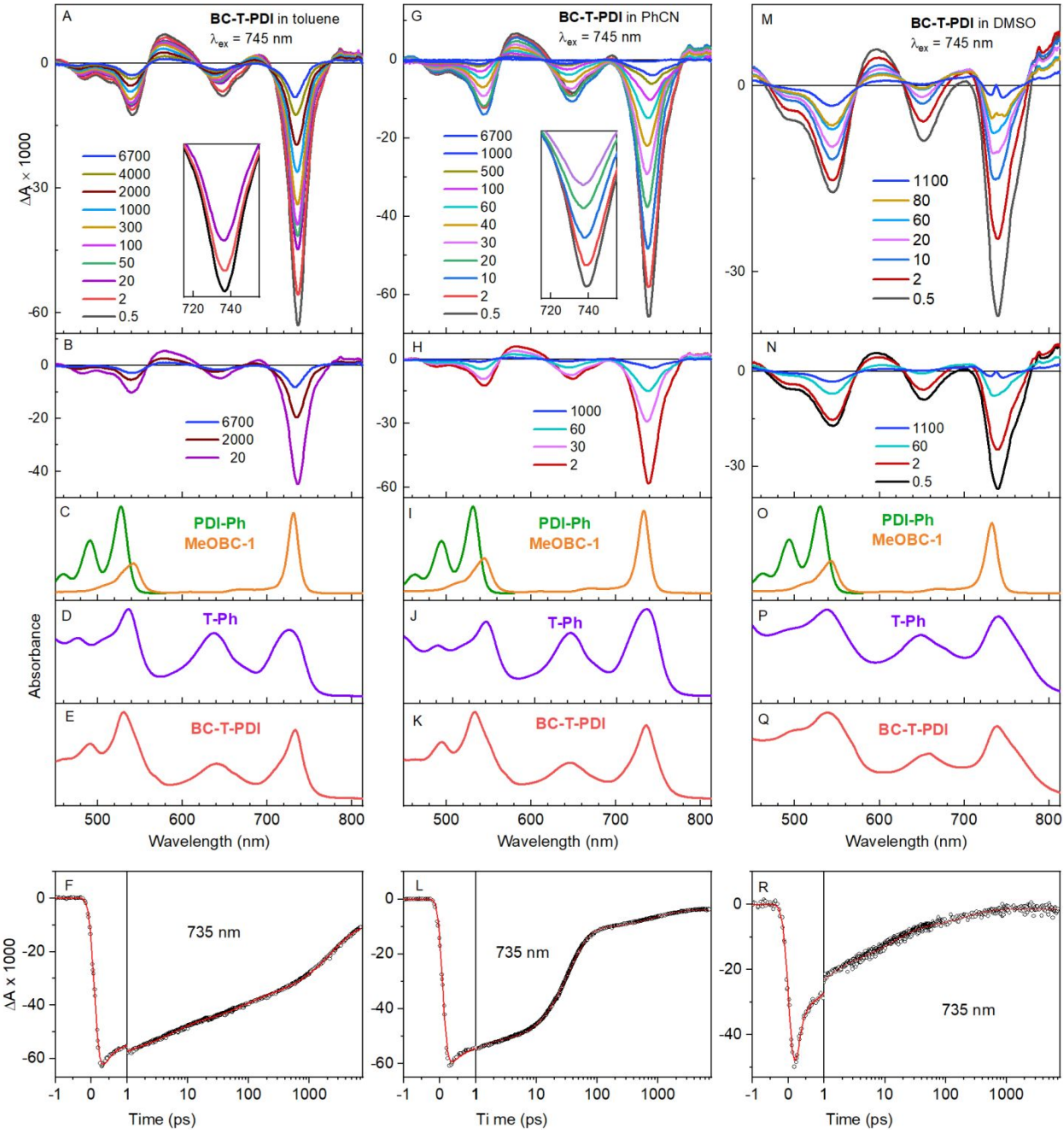

Figure 6. TA data for pentad **BC-T-PDI** in toluene (left), PhCN (middle), and DMSO (right). For each column of data, the top two panels show TA data at various times after excitation with a 100-fs flash at 745 nm; the middle three panels show ground-state absorption spectra of monomers **PDI-Ph** and **MeOBC-1**, benchmark triad **T-Ph** and the pentad; the bottom panel shows a kinetic profile for decay of combined $S_0 \rightarrow S_1$ bleaching and $S_1 \rightarrow S_0$ stimulated emission of the central panchromatic triad (T) of the pentad. The insets to panels A and G show evolution of this composite NIR feature at early times.

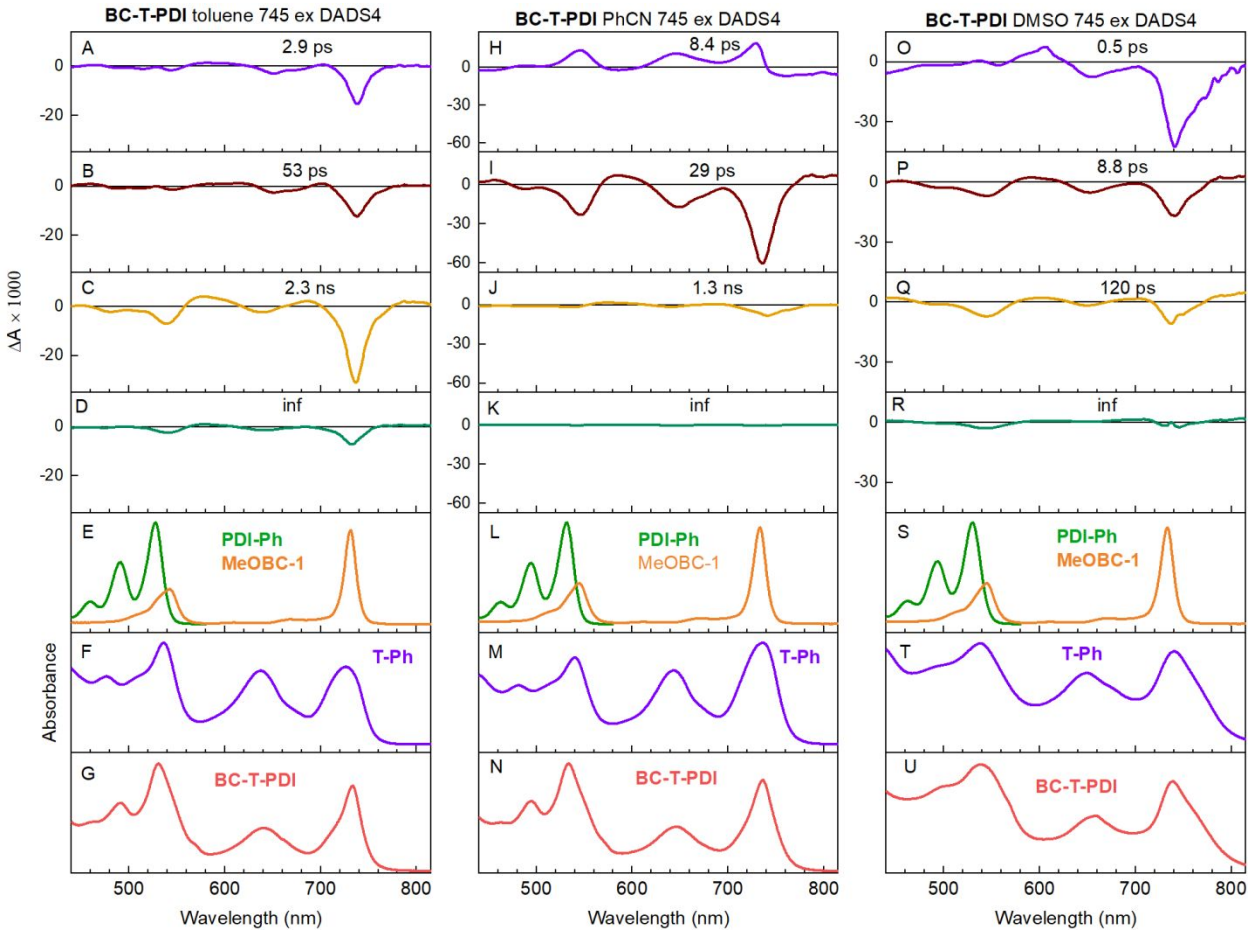

Figure 7. DADS summary for **BC-T-PDI** in toluene (left), PhCN (middle), and DMSO (right) obtained using λ_{ex} = 745 nm.

*TA studies of **BC-T-PDI** in toluene.* The very close energies (< 100 cm^{-1}) of the S_1 excited states of the bacteriochlorin (BC) and panchromatic triad (T) constituents of pentad **BC-T-PDI** were noted above. The spacing is less than thermal energy at room temperature (~210 cm^{-1}), so no matter which is lowest, equilibration between the two excited states must occur, including in competition with subsequent processes (*e.g.,* excited-state charge transfer in polar media). The 745-nm excitation flashes are absorbed basically exclusively by the T component of the pentad to generate state BC-T*-PDI. Subsequent energy transfer to the bacteriochlorin to produce state BC*-T-PDI likely gives a major contribution to the early-time dynamics in Figure 6A for **BC-T-PDI** in toluene and the ~3 ps DADS in Figure 7A. Relaxations (vibrational/conformational/solvent)

within the S_1 excited state(s) also likely contribute to the 3 ps and 50 ps components (Figure 7A and B), and have been observed previously on these time scales for pentads[60] **ZnC-T-PDI** and **C-T-PDI** and for monomeric bacteriochlorins.[68]

The subsequent dynamics (Figure 6A and B) and 2.3-ns kinetic component (Figure 7C) for **BC-T-PDI** in toluene have the characteristics of the S_1 excited state of the bacteriochlorin (BC*) along with some contribution from the excited triad (T*). This assignment derives from the wavelengths, widths, and relative intensities of the nominal Q_y bleach (plus stimulated emission) at ~740 nm and the nominal Q_x bleach at ~540 nm for the pentad (Figure 7C); these transient features can be compared with characteristics of the ground-state absorption bands of the benchmarks (Figures 7E–G). The 2.3-ns S_1 lifetime for **BC-T-PDI** in toluene is shorter than that for the **MeOBC-1** benchmark (5.2 ns) and is closer to that for benchmark triad **T-Ph** (2.0 ns) in toluene (Table 1). However, electronic interactions between the BC and T constituents of **BC-T-PDI** (mediated by the phenylethyne linker) may alter the S_1 properties of the pentad compared to those of the benchmarks (*vide infra*). Thus, both quantum-mechanical and thermal mixing of BC*-T-PDI and BC-T*-PDI give rise to collective properties of the S_1 excited state of the pentad, including a (mean) 2.3-ns S_1 lifetime.

The small-amplitude signals seen at long times (~7 ns) in Figures 6A and 6B, and the associated long-lived (∞) DADS (Figure 7D) observed after S_1 decay is complete, both have characteristics expected for the lowest triplet excited state of the bacteriochlorin constituent of **BC-T-PDI**, likely along with some contribution from the triplet excited state of the triad constituent. Collectively, the TA data for **BC-T-PDI** in toluene show no spectral or kinetic evidence for excited-state charge transfer.

*TA studies of **BC-T-PDI** in PhCN.* The TA data for **BC-T-PDI** in PhCN show in early-time dynamics (Figure 6G) an initial 8-ps kinetic component (Figure 7H) that likely reflects a

combination of BC-T*-PDI → BC*-T-PDI excited-state energy transfer, some back transfer to equilibrate to the two excited states, and associated vibrational/conformational/solvent relaxations within the S_1 states. The 29-ps DADS for **BC-T-PDI** in PhCN (Figure 7I) has basically the same shape (and amplitude) as the 2.3-ns component for this pentad in toluene (Figure 7C). The features are consistent with return of BC*-T-PDI to the ground state, likely involving excited-state hole/electron transfer to produce charge-separated intermediate BC^+-T^--PDI followed by rapid charge recombination.

Pentad **BC-T-PDI** in PhCN also shows a small 1.3-ns kinetic component that likely represents decay of BC-T*-PDI to the ground state (Figure 7J). The Q_y bleaching decay (~740 nm) is broader than for the 29-ps component, consistent with the relative widths of the ground-state Q_y absorption bands of benchmarks **T-Ph** (Figure 7M) and **MeOBC-1** (Figure 7L), respectively. The amplitude of the 1.3 ns component is ~15% of that of the 29-ps component and thus represents a minor decay pathway. The 1.3 ns time constant is comparable to the 1.4 ns lifetime for T* in benchmark triad **T-Ph** in PhCN (Table 1). However, it is unclear if this match is fortuitous given the multiple potential processes involved in the excited-state dynamics for the pentad in PhCN. Regardless, there is no evidence for formation of a long-lived full charge-separated state BC^+-T-PDI^-. In short, excited **BC-T-PDI** largely (80%) returns to the ground state by ~100 ps and decays completely by ~3 ns (Figures 6 and 7 and S8, S9 and S15).

*TA studies of **BC-T-PDI** in DMSO.* The DADS for **BC-T-PDI** in DMSO reveal characteristics that are different in detail from those for the pentad in PhCN. Before summarizing the observations, recall from Figure 4C that the Q_y ($S_0 \rightarrow S_1$) ground-state absorption band of the benchmark triad **T-Ph** is bathochromically shifted and broadened in DMSO compared to that in toluene (and PhCN). In comparison, the Q_y band of the benchmark bacteriochlorin **MeOBC-1** is relatively unaffected by solvent (Figure 4B). Thus, for pentad **BC-T-PDI** in DMSO, the energy

of the excited triad constituent may lie below that of the excited bacteriochlorin. Thus, the excited-state equilibrium favors BC-T*-PDI over BC*-T-PDI, or to the extent that quantum-mechanical mixing occurs, the S_1 excited state of the pentad has more T* than BC* character.

These insights are consistent with the fast dynamics (Figure 6M) and ~0.5 ps DADS (Figure 7O) for **BC-T-PDI** in DMSO. The spectrum has characteristics expected for decay of the Q_y bleach and stimulated emission associated with the disappearance of the excited triad BC-T*-PDI in the pentad (Figure 7O). The prominent 9-ps and the smaller 120-ps components have spectral characteristics that suggest the involvement of both the BC and T components, such as for charge-transfer intermediate BC^+-$T^–$-PDI. Perhaps there are several "conformers" of the pentad that differ in the relative orientations of the components about the linkers. The short lifetimes, particularly of the 9-ps component, suggest that charge recombination is even more rapid for the pentad in DMSO than in PhCN. The TA difference spectra at long times (Figure 6N) and small long-time (∞) DADS component (Figure 7R) have characteristics associated with the panchromatic triad, and may derive from the triplet excited state. The triplet state could be formed as a minor pathway for charge recombination of intermediate BC^+-$T^–$-PDI, the dominant route reforming the ground state.

Regardless of the assignments of the TA difference spectra, **BC-T-PDI** in DMSO shows even more rapid deactivation to the ground state than that of the pentad in PhCN or toluene. There is no evidence in any of the three solvents for the full charge-separated state BC^+-T-$PDI^–$. This state would exhibit bleaching of the PDI ground-state absorption bands at 495 and 530 nm (see Figures 7E, L and S) and appearance of the PDI anion absorption features at 715 and 810 nm. Such features were observed previously[60] in the TA difference spectrum for state ZnC^+-T-$PDI^–$ of the related pentad **ZnC-T-PDI** (Chart 1) in PhCN (~5% yield) and in DMSO (~30% yield) as

noted in the Introduction. These findings are discussed below, after presentation of relevant MO and excited-state characteristics of **BC-T-PDI** obtained from DFT and TDDFT calculations.

Molecular-orbital characteristics. Figure 8 presents the energies and electron-density distributions of the highest occupied MO (HOMO), the HOMO-1, the lowest unoccupied MO (LUMO) and the LUMO+1 for **BC-T-PDI** in toluene and DMSO obtained from DFT calculations. For comparison, Figure 8 also gives the characteristics of the analogous orbitals for pentads **ZnC-T-PDI** and **C-T-PDI** (in toluene) studied previously.[60] The energies of the orbitals from HOMO-5 to LUMO+5 for all three pentads are depicted in Figure S17. The electron-density distributions and energies for all orbitals from HOMO-11 to LUMO+11 for pentad **BC-T-PDI** in toluene and DMSO are shown in Tables S1 and S2, respectively. The orbital energies differ by up to ~0.15 eV in DMSO versus toluene dependent on whether the orbital primarily involves the BC, T, or PDI constituent. For comparison, the MOs for bacteriochlorin monomer **MeOBC-1** in toluene are given in Table S3.

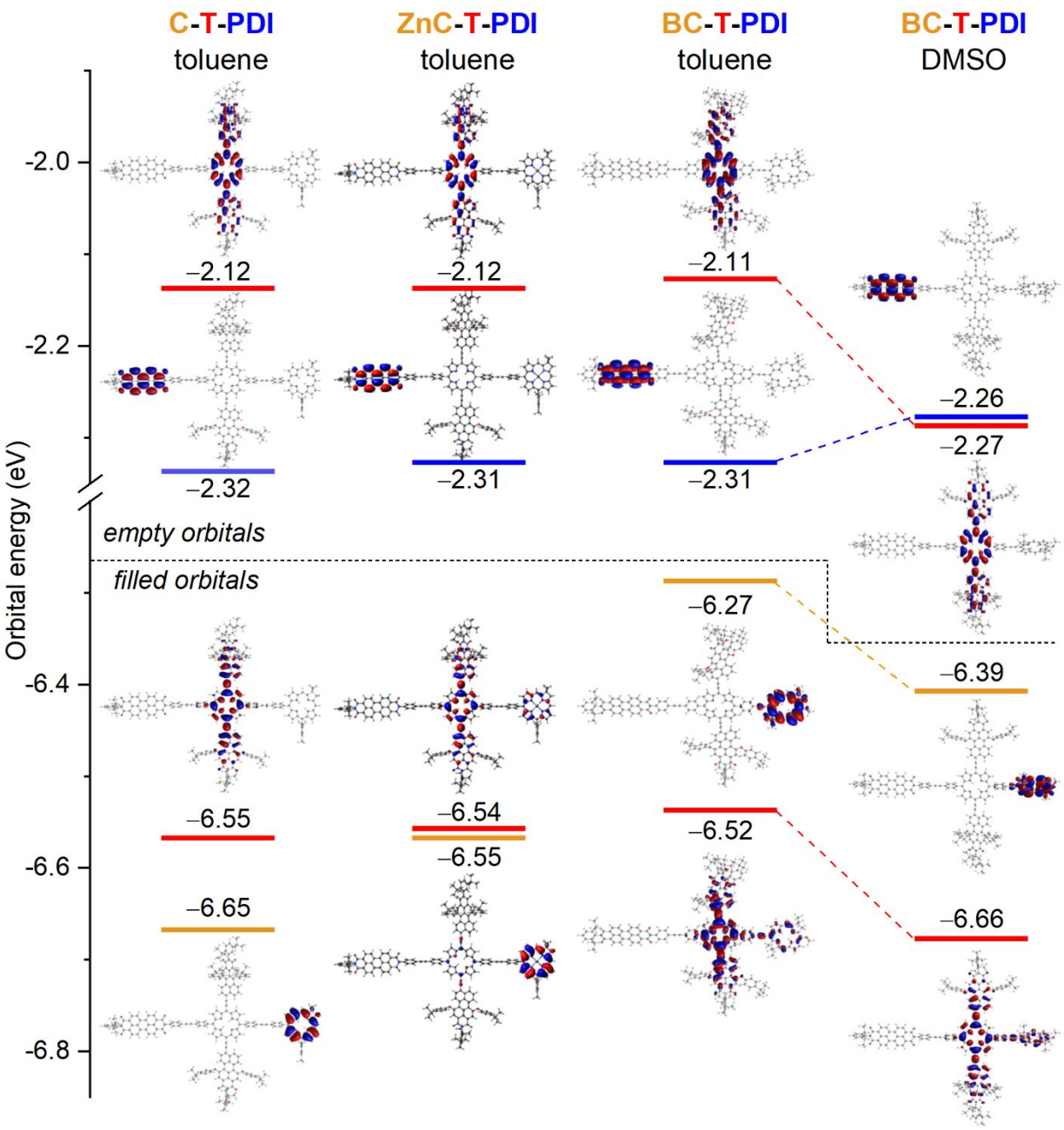

Figure 8. Frontier MO energies and electron-density distributions for pentads **ZnC-T-PDI** and **C-T-PDI** studied previously[60] and pentad **BC-T-PDI** studied here, in the solvents indicated. The lines at the MO energies are colored to match the constituent: (bacterio)chlorin (gold), perylene-diimide (blue), and central panchromatic triad (red). The MO images for **BC-T-PDI** in DMSO are rotated from those in toluene to show a face-on perspective of the central porphyrin of T.

There are two key insights from the MO data in Figure 8. (1) The LUMO of **BC-T-PDI** in toluene is on the PDI constituent, the next lowest empty orbital being 0.2 eV to higher energy

and residing on the central triad. In DMSO, the two orbitals have comparable energy due primarily to stabilization of the lowest empty orbital on the triad along with some destabilization of the empty orbital on PDI. A similar effect was noted previously for **ZnC-T-PDI** and **C-T-PDI** in DMSO vs toluene, supported by calculations on the benchmark triad **T-Ph** in the two solvents.[60] Thus, for the pentad **BC-T-PDI** in toluene, the MO characteristics and associated redox properties do not pose an impediment for photoinduced charge transfer leading to the electron ultimately residing on the terminal PDI. For **BC-T-PDI** in DMSO, an equilibrium likely exists between the electron residing on the PDI and T components. (2) The main motivation of this study was to facilitate the hole ending up on the opposite terminus of the charge-separation unit in the array, namely on the bacteriochlorin of **BC-T-PDI**. The logic underlying this design is readily seen from the upshift in the energy of this highest occupied orbital (gold in Figure 8) by 0.1 eV from –6.65 eV for **C-T-PDI** to –6.55 eV for **ZnC-T-PDI**, and by a more substantial shift of 0.28 eV to –6.27 eV in progressing to **BC-T-PDI** for the arrays in toluene. Similarly, in terms of MO characteristics (and derived redox properties), the hole could reside on the bacteriochlorin constituent for **BC-T-PDI** in DMSO (Figure 8).

For **C-T-PDI** in toluene, the chlorin HOMO lies 0.1 eV below that of the central triad, such that the hole will not shift from T^+ to C (Figure 8). The HOMO of the zinc chlorin of **ZnC-T-PDI** in toluene is basically degenerate with that of the central triad such that the hole can shift back and forth between the two. In the case of **BC-T-PDI,** the HOMO on the bacteriochlorin lies 0.25 eV above that for the central triad in toluene and 0.27 eV higher in DMSO. Thus, shifting a hole from T^+ to the BC is thermodynamically quite favorable (because BC is easier to oxidize than T). Thus, the yield of full charge separation for **BC-T-PDI** would be improved from that observed for **ZnC-T-PDI** in PhCN (~5%) and in DMSO (~30%). The fact that this was not found, as described above, suggests that the additional changes that accompany replacement of the zinc chlorin of

ZnC-T-PDI with the bacteriochlorin of **BC-T-PDI** more than counteract the more favorable oxidation of the terminal hole-acceptor (electron-donor) unit. These additional changes (excited-state energies and linker) have been noted above and are considered further in the following.

Calculated excited-state energies and absorption spectra. TDDFT calculations were performed on **BC-T-PDI** in toluene and DMSO to obtain the energies and electronic compositions of the excited states responsible for the absorption spectrum spanning the violet to red regions. The results for the first 16 excited states are given in Table S4 (toluene) and Table S5 (DMSO). Figures 9A (toluene) and 9B (DMSO) plot the calculated wavelengths and relative oscillator strengths of the transitions as colored sticks along with an overall spectrum (dashed blue) obtained by giving each transition a 10-nm Gaussian skirt. The calculated energies (wavelengths) were shifted to lower energy by 300 cm^{-1} to afford the best overall match with the measured spectrum (red) in toluene, and for consistency the same shift was used for the spectra in DMSO. The major features are identified as arising from absorption transitions associated with the bacteriochlorin (BC), panchromatic triad (T), or perylene-diimide (PDI) constituents of **BC-T-PDI**. Transitions dominated by the bacteriochlorin can be seen by comparison with the results of the TDDFT calculations given in Table S6 for monomer **MeOBC-1**. Other associations are derived as follows.

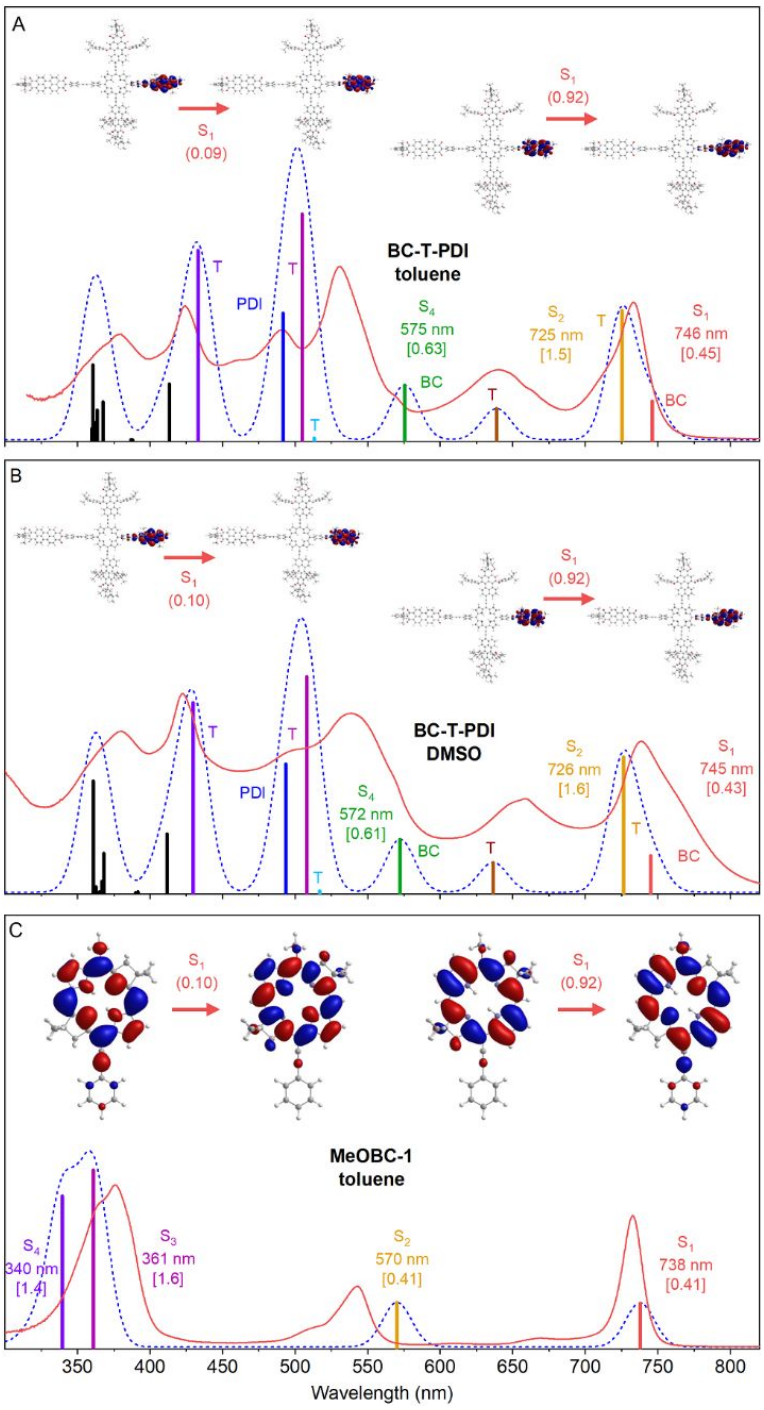

Figure 9. Absorption spectra calculated by TDDFT (colored sticks and blue dashed lines using 10-nm Gaussian skirts) are given along with pairs of occupied and virtual NTOs for absorption from S_0 to S_1 for pentad **BC-T-PDI** in toluene (A) and DMSO (B) and bacteriochlorin monomer **MeOBC-1** in toluene (C). The calculated spectra are shifted to lower energy by 300 cm^{-1} for **BC-T-PDI** and 200 cm^{-1} for **MeOBC-1** to best align with the measured spectrum (red solid line). The eigenvalue (weight) for each pair of NTOs that contributes to the transition is indicated in parenthesis. The calculated wavelength and oscillator strength (in square brackets) for various transitions are given at the bottom of each panel.

Tables S4 (toluene) and S5 (DMSO) show that each excited state for **BC-T-PDI** is derived from multiple (up to a dozen) one-electron promotions between the MOs shown in Tables S1 and S2. Thus, it is difficult to ascertain the net change in electron density that accompanies the absorption transition from the ground state to a given excited state. The natural transition orbitals (NTOs) provide a convenient way to visualize such electron-density changes.[69] An electronic excitation is viewed as a set of one-electron promotions from an occupied NTO to an empty NTO, each promotion weighted by an eigenvalue. The occupied and empty NTOs for a given transition are referred to as an NTO pair. The NTO pairs for the S_1 excited states for pentad **BC-T-PDI** are shown in Figures 9A (toluene) and 9B (DMSO). The NTO pairs associated with excited states S_1 – S_8 along with the measured and calculated spectra for **BC-T-PDI** in toluene are given in Figures S18– S21. The NTO pairs associated with excited states S_1 – S_4 along with the measured and calculated spectra for **MeOBC-1** in toluene are given in Figure S22. The full set of NTO pairs for the first 16 excited states is presented for **BC-T-PDI** in toluene and DMSO and for **MeOBC-1** in toluene in Tables S7–S9.

Figures 9A and 9B show that the lowest singlet excited state of **BC-T-PDI** in toluene is associated with the bacteriochlorin. This $S_0 \rightarrow S_1$ transition has an oscillator strength of f = 0.45 and involves two NTO pairs with 0.92/0.09 weighting. Similar characteristics are observed for the bacteriochlorin monomer **MeOBC-1** (Figure 9C). [The eigenvalues for the NTO pairs in some cases do not sum precisely to unity because of the minor emissive contributions.] The energy of this BC*-T-PDI excited state is calculated to lie ~390 cm^{-1} below the S_2 excited state, which is the lowest excited state of the PMI-P-PMI panchromatic triad (BC-T*-PDI). The electron-density changes in the S_2 state (relative to S_0) are located primarily on the central porphyrin of the triad. Higher excited states of the PMI-P-PMI triad have electron-density changes on the two perylene-monoimides, the porphyrin, or both (Figures S18–S20 and Tables S4 and S5).

The prediction that BC*-T-PDI lies lower than BC-T*-PDI for **BC-T-PDI** in toluene is consistent with the ground-state absorption and fluorescence data (Figures 4 and 5) and TA data (Figures 6 and 7). As discussed above, the data indicate that the two states are closer in energy ($\leq$100 cm^{-1}) than shown by the calculations (390 cm^{-1}), but the agreement is good. Also, as noted above, the data suggest that the ordering of the two excited states reverses for the two pentads in DMSO due to the solvent effect on the spectrum of the panchromatic triad as exemplified by benchmark **T-Ph** (Figure 4). However, the TDDFT calculations predict that BC*-T-PDI remains the lowest singlet excited state of **BC-T-PDI** in DMSO (Figure 9B and Table S5). Perhaps there are specific interactions between the DMSO solvent molecules and the constituents of **BC-T-PDI** that are not captured in the polarizable continuum solvent model used in the TDDFT calculations.

Figures 9A and 9B demonstrate the overall good agreement between the calculated and measured spectrum for pentad **BC-T-PDI** in toluene. This includes the contributions of the panchromatic triad, which shows an intense (f = 1.5) red region band and other features of comparable intensity across the violet-red visible spectrum. The predicted oscillator strengths and electronic compositions of the features derived from the T component of **BC-T-PDI** are virtually identical to those obtained previously for a PMI-P-PMI triad with structure similar to the **T-Ph** benchmark.[70] Also noteworthy is that the $S_0 \rightarrow S_1$ (Q_y) band associated with the BC component of the pentad in toluene or DMSO (745–646 nm; f = 0.43–0.45) is less intense than the nominal Q_x feature (572–575 nm; f = 0.61–0.63), which gives rise to absorption to the S_4 excited state of the pentad (Figures 9A and 9B, green). Normally, the Q_y band of bacteriochlorins is much more intense than the Q_x band. The difference here reflects in part the effects on the bacteriochlorin of the directly attached ethyne of the phenylethyne group, which is the linker to the central porphyrin. This can be seen by comparison with Figure 9C for ethyne-bearing monomer **MeOBC-1** (Scheme 1), which shows that the S_1 and S_2 transitions have similar oscillator strength (0.41). The fact that

the oscillator strength for the $S_0 \rightarrow S_2$ transition in **BC-T-PDI** increases to ~0.6 indicates the presence of linker-mediated interactions between the bacteriochlorin (BC) and panchromatic triad (T) constituents of the pentad.

Balancing energetics and electronic interactions. Figure 10 shows a state diagram for the new pentad **BC-T-PDI** (Chart 2) described herein along with those for prior[60] analogues **ZnC-T-PDI** and **C-T-PDI** (Chart 1). These diagrams were constructed using the absorption spectra (*e.g.,* Figure 3) and MO energies (*e.g.,* Figures 8 and S17) for the pentads and benchmarks, and redox properties of benchmarks and related tetrapyrroles and perylenes.[60]

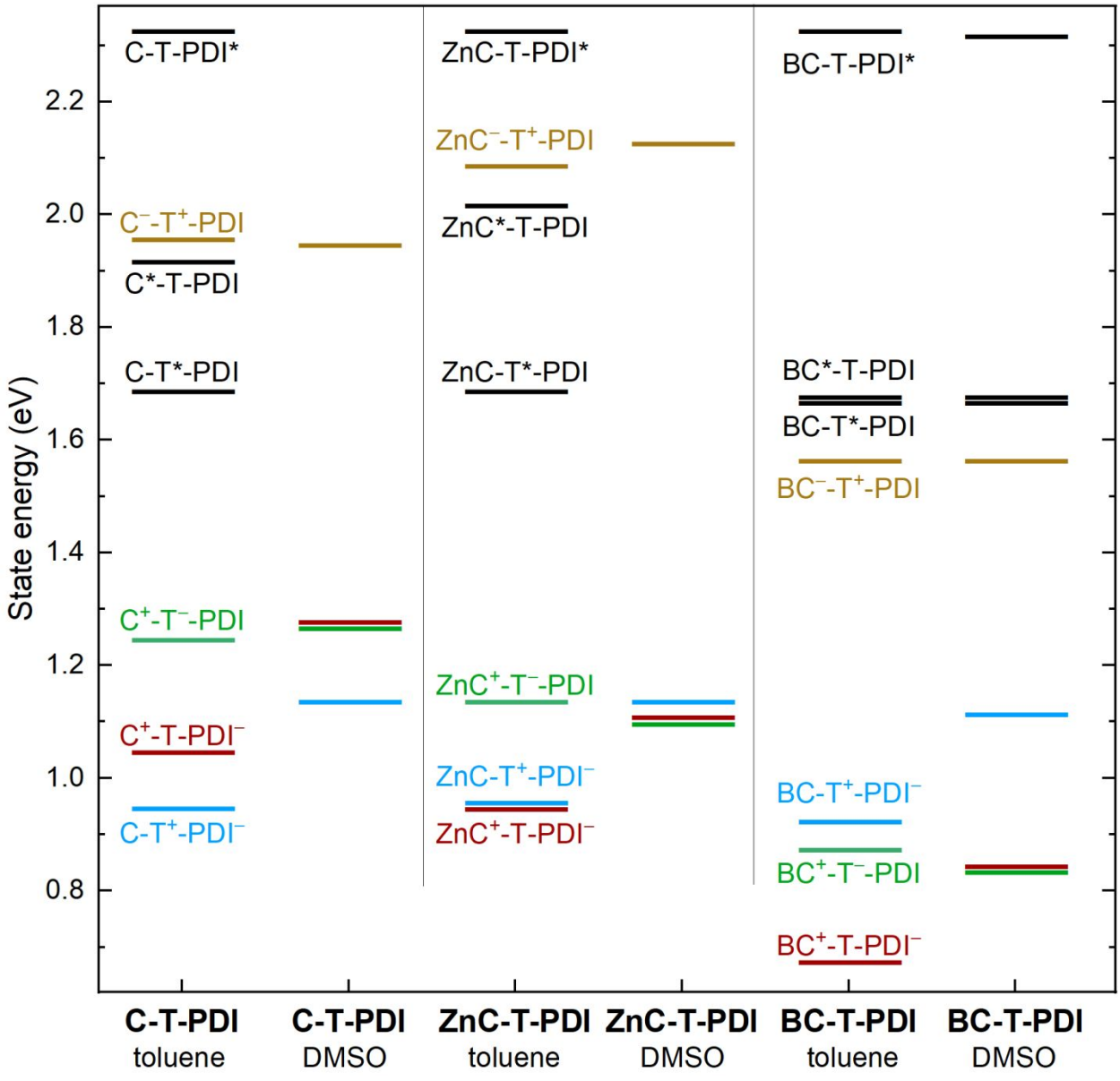

Figure 10. State diagrams showing energies of excited states (black), charge-separated intermediates (gold, green, blue), and full charge-separated state (brown) involving the constituents of triads **C-T-PDI** and **ZnC-T-PDI** studied previously[60] (Chart 1) and **BC-T-PDI** studied here (Chart 2), in toluene and DMSO.

The design of **BC-T-PDI** entailed several criteria so that – compared to **C-T-PDI** and **ZnC-T-PDI** in toluene, PhCN, and DMSO – the new pentad would exhibit (1) comparable or improved panchromatic absorption and (2) a higher yield of the long-lived full charge-separated state. The principal considerations were as follows.

The primary motivation was to utilize the more easily oxidized bacteriochlorin as the terminal hole acceptor (or electron donor) in place of the free base or zinc chlorin. The rationale is evident in the above-noted progressive upshift in the energy of the HOMO of the terminal acceptor (C < ZnC < BC) in Figure 8 (gold) and companion stabilization of the full charge-separated state (C^+-T-PDI^- > ZnC^+-T-PDI^- > BC^+-T-PDI^-) in Figure 10 (brown).

The second criterion was to choose a substituent pattern on the bacteriochlorin, within the constraints of current synthesis methodology, so that the lowest singlet excited state of the bacteriochlorin (BC*-T-PDI) would lie above that of the PMI-P-PMI panchromatic triad (BC-T*-PDI). Synthesis considerations led to the use of a phenylethyne linker from the BC unit to the central porphyrin of T because such a design required only a single Sonogashira coupling, whereas a diphenylethyne would require both a Suzuki reaction and a Sonogashira reaction, a sequence that to date has proved difficult with the present bacteriochlorin building blocks. That longer linker was used previously[60] to connect the free base chlorin of **C-T-PDI** or the zinc chlorin of **ZnC-T-PDI** to the central porphyrin of the panchromatic triad (Chart 1).

Known design features influenced the choice of architecture: (1) attachment of the ethynyl moiety of a phenylethyne group to a *meso*-position of a bacteriochlorin results in a ~20 nm bathochromic shift in the Q_y band, with the exact amount depending on the nature and patterns of

other substituents;[71] and (2) the presence of a *meso*-methoxy group on an unsubstituted (other than the pair of geminal dimethyl groups) bacteriochlorin gives an ~5 nm hypsochromic shift of the Q_y band, whereas that shift can approach ~30 nm depending on the other substituents.[72] Using the known 713-nm position of the "unsubstituted" bacteriochlorin,[72] these factors suggested that the bacteriochlorin Q_y band would be close to the nominal Q_y band (~725–740 nm depending on solvent; Figure 5D) of the panchromatic triad and thus that the corresponding excited states BC*-T-PDI and BC-T*-PDI would be close in energy.

The desired outcome was that BC*-T-PDI would lie above BC-T*-PDI such that all energy harvested by the BC and PDI constituents of **BC-T-PDI** would get funneled to the triad to generate BC-T*-PDI. Obviously, that same excited state is produced directly by the panchromatic absorption of the core triad itself. As noted above, the static and time-resolved spectral data show that BC*-T-PDI lies slightly below BC-T*-PDI in toluene (supported by TDDFT calculations) and PhCN, but the reverse appears to be the case for the pentad in DMSO. The two excited states are sufficiently close in energy that they are likely in thermal equilibrium. Regardless, whether BC*-T-PDI or BC-T*-PDI is the lowest energy singlet excited state should not limit formation of the long-lived charge-separated state BC^+-T-$PDI^–$. That state is far lower than the charge-separated intermediates such as BC^+-$T^–$-PDI and BC-T^+-$PDI^–$, as shown in Figure 10. That figure also shows that this most favorable state ordering was not the case for pentads **C-T-PDI** and **ZnC-T-PDI** due to the lower energy HOMO (and higher oxidation potential) of C or ZnC compared to that of BC.

The Φ_f and τ_S results (Table 1) and TA data (Figures 6 and 7) reveal near quantitative excited-state quenching by hole/electron transfer for **BC-T-PDI** in PhCN and DMSO. If BC*-T-PDI is lowest, excited-state hole/electron transfer would predominantly produce intermediate BC^+-$T^–$-PDI. The alternative initial product $BC^–$-T^+-PDI is much higher in energy and only slightly below BC*-T-PDI; its formation would have a much less favorable Franck-Condon factor. If BC-

T*-PDI is lowest, excited-state hole/electron transfer would again produce BC^{+}-T^{-}-PDI, along with BC-T^{+}-PDI^{-}. The two charge-separated intermediates are expected to lie relatively close in energy and thus have similar free energy gaps (ΔG) from BC-T*-PDI (Figure 10). Assuming similar reorganization energies (λ), the Franck-Condon factors would be similar for the two excited-state charge-transfer processes, BC-T*-PDI $\rightarrow$ BC^{+}-T^{-}-PDI and BC-T*-PDI $\rightarrow$ BC-T^{+}-PDI^{-}, which in the Marcus formulation depend on the relationship between ΔG and λ. However, the BC-T*-PDI $\rightarrow$ BC^{+}-T^{-}-PDI process is expected to have a much greater rate constant than that for BC-T*-PDI $\rightarrow$ BC-T^{+}-PDI^{-} because of the difference in electronic coupling factors. In particular, the BC and T (PMI-P-PMI) units of the pentad are joined by a phenylethyne linker whereas the T and PDI units are joined by the longer diphenylethyne linker (Chart 2). Prior work has shown that energy and charge-transfer between tetrapyrroles joined by a phenylethyne linker are significantly faster than for diphenylethyne-linked analogues.[73]

These considerations indicate that regardless of whether BC*-T-PDI or BC-T*-PDI is the lowest singlet excited state of the pentad, excited-state hole/electron transfer is expected to primarily produce charge-separated intermediate BC^{+}-T^{-}-PDI. This conclusion is supported by the TA data described above. Namely, there is no indication of transient reduction of PDI with associated bleaching of the PDI ground-state absorption bands and appearance of the PDI anion bands. Instead, the transient states primarily involve the BC and T components (*i.e.,* BC^{+}-T^{-}-PDI).

The greater electronic coupling between T and BC units (mediated by the phenylethyne linker) compared to the coupling between the T and PDI units (mediated by the longer diphenylethyne linker) that favors the excited-state hole/electron transfer BC-T*-PDI $\rightarrow$ BC^{+}-T^{-}-PDI versus BC-T*-PDI $\rightarrow$ BC-T^{+}-PDI^{-} has implications for the subsequent competitive ground-state hole/electron-transfer processes. In particular, once BC^{+}-T^{-}-PDI is formed by excited-state hole/electron transfer, a ground-state electron (or hole) shift process BC^{+}-T^{-}-PDI $\rightarrow$ BC^{+}-T-PDI^{-}

across the diphenylethyne linker is required to produce the full charge-separated state. In competition is the charge-recombination process BC^{+}-T^{-}-PDI → BC-T-PDI that involves ground-state hole/electron transfer across the shorter phenylethyne linker. The greater electronic coupling for charge recombination affords a larger rate constant than that for the electron-shift process. This difference in electronic coupling for the competitive decay routes for BC^{+}-T^{-}-PDI is likely more substantial than differences in Franck-Condon (ΔG vs λ) factors in causing deactivation rather than formation of the full charge-separated state.

In the prior studies of **C-T-PDI** and **ZnC-T-PDI**, the analogous charge recombination and hole/electron-shift processes had similar electronic coupling (both mediated by diphenylethyne linkers). Thus, the effect of zincation of the chlorin terminal hole acceptor and increased solvent polarity appeared to be key in slowing charge-recombination (via a less favorable ΔG vs λ relationship) sufficiently to allow the full charge-separated state to form with ~30% yield for **ZnC-T-PDI** in DMSO. Here, for **BC-T-PDI**, despite much more favorable energetics for charge separation designed into the array, enhanced electronic coupling for charge-recombination appears to undermine the desired full charge separation across the array.

Conclusion and outlook

A new integrated array containing a perylene-monoimide–porphyrin–perylene-monoimide (panchromatic absorber), a bacteriochlorin (hole-acceptor / electron-donor), and a perylene-diimide (electron acceptor) provides enhanced light-harvesting but only partial charge transfer. Static and time-resolved optical studies show that pentad **BC-T-PDI** exhibits near-quantitative quenching of the S_1 excited state of the array in PhCN and DMSO, followed by rapid charge recombination of intermediate BC^{+}-T^{-}-PDI with no observable formation of the full charge-separated state BC^{+}-T-PDI^{-}. Analysis of the electronic properties of the array indicate that

although the bacteriochlorin in the pentad gives move favorable energetics for oxidation of this terminal hole acceptor unit than prior analogues, significant electronic coupling between that unit and the central panchromatic triad facilitates charge recombination thereby precluding full charge separation across the architecture. On the basis of these findings, a next-generation design is to replace the phenylethyne with a diphenylethyne linker between the bacteriochlorin terminal hole acceptor and the central porphyrin of the bis(perylene-monoimide)porphyrin panchromatic absorber. This will require advances in synthetic methodology to allow access to the necessary synthesis intermediates in sufficient quantity for production of pentad arrays.

Experimental Section

General methods. ^{1}H NMR and ^{13}C NMR spectra were collected at room temperature in $CDCl_3$ unless noted otherwise. Silica (40 μm average particle size) was used for column chromatography. THF was freshly distilled from sodium/benzophenone. All other solvents (anhydrous or reagent-grade) were employed as received from commercial suppliers. Commercial compounds were used as received. Noncommercial compounds **MeOBC-Br**[62] and **PDI-T-e**[59] were prepared following literature procedures.

Typical procedure for purification of pentads. After the completion of reaction, the reaction mixture was allowed to cool to room temperature and then concentrated *in vacuo*. The resulting crude mixture was purified by SEC using BioRad Bio-Beads SX-1 (THF) to remove tetrapyrrole monomers and other oligomers. Then eluant collected from SEC was then passed through a short silica pad to remove materials derived from the SEC resin, thereby affording the pure pentad.

Analytical size exclusion chromatography. Analytical SEC was performed to monitor the reaction and purification of the samples.[66] Analytical SEC columns (styrene-divinylbenzene copolymer) were purchased from Polymer Laboratories. Analytical SEC was performed with an Agilent 1100 HPLC using PLgel 100 Å, PLgel 500 Å and PLgel 1000 Å in series eluting with freshly distilled THF (flow rate = 0.6 mL/min) at 30 °C. Sample detection was achieved by absorption spectroscopy using a diode array detector with quantitation at 431, 530, 640 and 730 nm, which best captures the peaks of the array **BC-T-PDI**.

Absorption and fluorescence spectra. Absorption spectra were measured using dilute solutions of the compounds in UV-transparent cuvettes versus a solvent blank. All data reported herein were obtained at room temperature.

5,15-Bis[2-(3,4-(*N*-(2,6-diisopropylphenyl)iminodicarbonyl)-1,6-bis(4-*tert*-butyl-phenoxy)perylene-9-yl)ethynyl]-10-[4-(2-(4-(9,10-(*N*-(2,6-diisopropylphenyl)iminodi-carbonyl)perylene-3,4-dicarboximido)phenyl)ethynyl)phenyl]-20-[4-(2-(15-methoxy-8,8,18,18-tetramethylbacteriochlorin-5-yl)ethynyl)phenyl]porphyrin (BC-T-PDI). Following a general procedure[59] with modification, a solution of **MeOBC-Br** (2.0 mg, 4.2 μmol) and **PDI-T-e** (2.0 mg, 0.73 μmol) in toluene/TEA (2.4 mL, 5:1) was degassed by four freeze/pump/thaw cycles. A sample of $Pd(PPh_3)_4$ (2.0 mg, 1.7 μmol) was then added, and the resulting mixture was stirred 12 h at 60 °C. The mixture was allowed to cool to room temperature, concentrated and purified by SEC (THF) to afford a brown solid (1.5 mg, 65%): λ_{abs} (THF) 376, 420, 488, 526, 638, 731 nm; t = 30.9 min; MALDI-MS for $C_{215}H_{175}N_{12}O_{13}$ $(M + H)^+$, calcd 3132.3396, found 3132.728 in the presence of α-cyano-4-hydroxycinnamic acid as matrix. NMR spectra could not be obtained due to solubility limitations.

5-Methoxy-15-(2-phenylethynyl)-8,8,18,18-tetramethylbacteriochlorin (MeOBC-1). Following a general procedure[65] with modification, a solution of **MeOBC-Br** (2.0 mg, 4.2 μmol) and phenylacetylene (10.0 μL, 91 μmol) in toluene/TEA (2.4 mL, 5:1) was degassed by four freeze/pump/thaw cycles. A sample of $Pd(PPh_3)_4$ (3.0 mg, 2.6 μmol) was then added, and the resulting mixture was stirred 12 h at 70 °C. The mixture was allowed to cool to room temperature, then concentrated and chromatographed [silica, hexanes/CH_2Cl_2 (3:1 to 1:1)]. The resulting crude product was further purified by two SEC (toluene) columns to afford a pink solid (1.3 mg, 62%): ^{1}H NMR (700 MHz) δ −1.86 (s, 1H), −1.59 (s, 1H), 1.96 (s, 6H), 1.97 (s, 6H), 4.36 (s, 2H), 4.47 (s, 3H), 4.62 (s, 2H), 7.43–7.47 (m, 1H), 7.50–7.54 (m, 2H), 7.90 (d, J = 7.4 Hz, 2H), 8.61–8.67 (m, 3H), 8.72–8.75 (m, 1H), 8.87–8.90 (m, 1H), 9.13–9.16 (m, 1H); ^{13}C{^{1}H} NMR (175 MHz) δ 31.0, 31.5, 45.1, 45.8, 47.4, 52.2, 65.2, 91.9, 95.2, 97.5, 98.6, 117.9, 120.7, 121.6, 123.5, 124.5, 128.0, 128.6, 131.5, 135.8, 136.1, 138.4, 153.4, 162.8; ESI-MS for $C_{33}H_{32}N_4O$ $(M + 2H)^{2+}$, calcd 251.1361 obsd 251.1358; λ_{abs} (toluene) 375, 541, 731 nm.

Photophysical properties. Static absorption (Shimadzu UV-1800), static emission (Horiba Nanolog), and other measurements were performed at room temperature on dilute (μM), Ar-purged solutions of compounds in toluene, PhCN, or DMSO. Determination of Φ_f values utilized samples with A ≤ 0.1 at the excitation wavelength and used *meso*-tetraphenylporphyrin in

non-degassed toluene ($\Phi_f = 0.070$)[67] as a standard. Values for τ_s and other excited-state processes including energy and charge transfer were probed using an ultrafast laser system with (0.5–1 μJ) ~100 fs excitation flashes at various wavelengths from a 1 kHz Ti:sapphire laser system with an optical parametric amplifier (Spectra Physics) and Helios/EOS TA spectrometer (Ultrafast Systems). Singlet lifetimes were also acquired in some cases via TCSPC using a Simple-Tau 130 system (Becker & Hickl) with an ~300 ps instrument response function. The TA data were analyzed using a combination of Surface Xplorer (Ultrafast Systems), CarpetView (Light Conversion), and custom fitting routines developed in OriginPro (OriginLab).

Density functional theory calculations. DFT calculations were performed with Gaussian 09 version E.01.[74] Calculations used the PCM model for the arrays in toluene. Molecular geometries were fully optimized using the hybrid B3LYP functional and the basis set 6-31G*. These calculations used Gaussian defaults with the exception of keyword Int=(Grid=Ultrafine,Acc2E=12). Electron-density distributions and energies of the molecular orbitals (MOs) were obtained using the long-range corrected ωB97XD functional and the basis set 6-31++G**. Some calculations were performed using Gaussian 16. To make the results of these calculations comparable to those run using Gaussian 09, the keyword G09Defaults was used in addition to the above mentioned keywords.

Acknowledgements

This work was supported by a grant from the Division of Chemical Sciences, Geosciences, and Biosciences, Office of Basic Energy Sciences of the U.S. Department of Energy (DE-FG02-05ER15661).

ASSOCIATED CONTENT

Supplementary Information

Transient-absorption difference spectra, decay associated difference spectra and analysis; molecular orbital energies and images; and excited-state properties from TDDFT calculations.

AUTHOR INFORMATION

Corresponding Authors

Email: jlindsey@ncsu.edu Tel: 919-515-6406

Email: david.bocian@ucr.edu Tel: 951-827-3660

E-mail: holten@wustl.edu Tel: 314-935-6480

Notes

The authors declare no competing financial interest.

References

1 A. A. Krasnovsky, *Biophys. J.,* 1972, **12**, 749–763.

2 G. Porter and M. D. Archer, *Interdiscip. Sci. Rev.,* 1976, **1**, 119–143.

3 D. Mauzerall, *Brookhaven Symp. Biol.,* **1977**, *28*, 64–73.

4 D. Mauzerall, in *Light-Induced Charge Separation in Biology and Chemistry*, ed. H. Gerischer and J. J. Katz, Berlin: Dahlem Konferenzen, Verlag-Chemie, Weinheim, 1979, vol. 12, pp. 241–257.

5 A. Harriman and J. Barber, in *Photosynthesis in Relation to Model Systems. Topics in Photosynthesis*, ed. J. Barber, Elsevier/North-Holland Biomedical Press, NY, 1979, vol. 3, ch. 8, pp. 243–280.

6 M. Calvin, *Energy Res.,* 1979, **3**, 73–87.

7 P. Cuendet and M. Grätzel, *Experientia,* 1982, **38**, 223–228.

8 S. G. Boxer, *Biochim. Biophys. Acta,* 1983, **726**, 265–292.

9 H. T. Tien, *Prog. Surf. Sci.,* 1985, **19**, 169–274.

10 D. Mauzerall and N. L. Greenbaum, *Biochim. Biophys. Acta*, 1989, **974**, 119–140.

11 D. Dolphin, J. Hiom and J. B. Paine III, *Heterocycles,* 1981, **16**, 417–447.

12 M. R. Wasielewski, *Photochem. Photobiol.,* 1988, **47**, 923–929.

13 D. Gust and T. A. Moore, *Science,* 1989, **244**, 35–41.

14 V. V. Borovkov, R. P. Evstigneeva, L. N. Strekova and E. I. Filippovich, *Russ. Chem. Rev.,* 1989, **58**, 602–619.

15 K. Maruyama and A. Osuka, *Pure Appl. Chem.,* 1990, **62**, 1511–1520.

16 D. Gust and T. A. Moore, *Adv. Photochem.,* 1991, **16**, 1–65.

17 D. Gust and T. A. Moore, *Top. Curr. Chem.,* 1991, **159**, 103–151.

18 M. R. Wasielewski, in *Chlorophylls*, ed. H. Scheer, CRC Press, Boca Raton, FL, 1991, pp. 269–286.

19 M. R. Wasielewski, *Chem. Rev.,* 1992, **92**, 435–461.

20 D. Gust, T. A. Moore and A. L. Moore, *Acc. Chem. Res.,* 1993, **26**, 198–205.

21 S. E. Gribkova, R. P. Evstigneeva and V. N. Luzgina, *Russ. Chem. Rev.,* 1993, **62**, 963–979.

22 K. Maruyama, A. Osuka and N. Mataga, *Pure Appl. Chem.,* 1994, **66**, 867–872.

23 H. Kurreck and M. Huber, *Angew. Chem. Int. Ed.,* 1995, **34**, 849–866.

24 A. Osuka, N. Mataga and T. Okada, *Pure Appl. Chem.,* 1997, **69**, 797–802.

25 D. Gust, T. A. Moore and A. L. Moore, *Pure Appl. Chem.,* 1998, **70**, 2189–2200.

26 J. Wojaczyński, L. Latos-Grażyński, P. J. Chmielewski, P. Van Calcar and A. L. Balch, *Inorg. Chem.,* 1999, **38**, 3040–3050.

27 D. Gust and T. A. Moore, in *The Porphyrin Handbook*, ed. K. M. Kadish, K. M. Smith and R. Guilard, Academic Press, San Diego, CA, 2000, vol. 8, pp. 153–190.

28 D. Gust, T. A. Moore and A. L. Moore, *Acc. Chem. Res.,* 2001, **34**, 40–48.

29 A. K. Burrell, D. L. Officer, P. G. Plieger and D. C. Reid, *Chem. Rev.,* 2001, **101**, 2751−2796.

30 N. Aratani, A. Tsuda and A. Osuka, *Synlett*, 2001, 1663–1674.

31 N. Aratani and A. Osuka, *Macromol. Rapid Commun.,* 2001, **22**, 725–740.

32 D. Holten, D. F. Bocian and J. S. Lindsey, *Acc. Chem. Res.,* 2002, **35**, 57–69.

33 J. Barber, J. M. Anderson, T. A. Moore, A. L. Moore and D. Gust, *Phil. Trans. R. Soc. Lond. B,* 2002, **357**, 1481–1498.

34 D. Kim and A. Osuka, *J. Phys. Chem. A,* 2003, **107**, 8791–8816.

35 N. Aratani and A. Osuka, *Chem. Rec.,* 2003, **3**, 225–234.

36 P. D. Harvey, in *The Porphyrin Handbook*, ed. K. M. Kadish, K. M. Smith and R. Guilard, Academic Press, San Diego, CA, 2003, vol. 18, pp. 63–250.

37 D. Kim and A. Osuka, *Acc. Chem. Res.,* 2004, **37**, 735–745.

38 H. Imahori, *J. Phys. Chem. B,* 2004, **108**, 6130–6143.

39 Z. S. Yoon, M.-C. Yoon and D. Kim, *J. Photochem. Photobiol. C: Photochem. Rev.,* 2005, **6**, 249–263.

40 Y. Kobuke, *Struct. Bond.,* 2006, **121**, 49–104.

41 E. Iengo, F. Scandola and E. Alessio, *Struct. Bond.,* 2006, **121**, 105–143.

42 Y. Nakamura, N. Aratani and A. Osuka, *Chem. Soc. Rev.,* 2007, **36**, 831–845.

43 P. C. Lo, X. Leng and D. K. P. Ng, *Coord. Chem. Rev,.* 2007, **251**, 2334–2353.

44 L. Flamigni, *J. Photochem. Photobiol. C: Photochem. Rev.,* 2007, **8**, 191–210.

45 A. Satake and Y. Kobuke, *Org. Biomol. Chem.,* 2007, **5** , 1679–1691.

46 P. D. Harvey, C. Stern, C. P. Gros and R. Guilard, *Coord. Chem. Rev.,* 2007, **251**, 401–428.

47 N. Aratani, D. Kim and A. Osuka, *Acc. Chem. Res.,* 2009, **42**, 1922–1934.

48 I. A. Maretina, *Russ. J. Gen. Chem.,* 2009, **79**, 1544–1581.

49 N. Aratani and A. Osuka, in *Handbook of Porphyrin Science*, ed. K. M. Kadish, K. M. Smith and R. Guilard, World Scientific Publishing Co., Singapore, 2010, vol. 1, pp. 1–132.

50 F. D'Souza and O. Ito, in *Handbook of Porphyrin Science*, ed. K. M. Kadish, K. M. Smith and R. Guilard, World Scientific Publishing Co., Singapore, 2010, vol. 1, pp. 307–437.

51 Z. S. Yoon, J. Yang, H. Yoo, S. Cho and D. Kim, in *Handbook of Porphyrin Science*, ed. K. M. Kadish, K. M. Smith and R. Guilard, World Scientific Publishing Co., Singapore, 2010, vol. 1, pp. 439–505.

52 S. Fukuzumi, in *Handbook of Porphyrin Science*, ed. K. M. Kadish, K. M. Smith and R. Guilard, World Scientific Publishing Co., Singapore, 2010, vol. 10, pp. 183–243.

53 P. D. Harvey, C. Stern and R. Guilard, in *Handbook of Porphyrin Science*, ed. K. M. Kadish, K. M. Smith and R. Guilard, World Scientific Publishing Co., Singapore, 2011, vol. 11, pp. 1–179.

54 J. Yang, M.-C. Yoon, H. Yoo, P. Kim and D. Kim, *Chem. Soc. Rev.,* 2012, **41**, 4808–4826.

55 T. Tanaka and A. Osuka, *Chem. Soc. Rev.,* 2015, **44**, 943–969.

56 N. Aratani and A. Osuka, *Bull. Chem. Soc. Jpn.,* 2015, **88**, 1–27.

57 M. Y. Wani, A. Balakrishna, S. Kumar and A. J. F. N. Sobral, *Curr. Org. Chem.,* 2015, **19**, 599–651.

58 H. Jing, J. Rong, M. Taniguchi and J. S. Lindsey, *Coord. Chem. Rev.,* 2022, **456**, 214278.

59 G. Hu, H. S. Kang, A. K. Mandal, A. Roy, C. Kirmaier, D. F. Bocian, D. Holten and J. S. Lindsey, *RSC Adv.,* 2018, **8**, 23854–23874.

60 A. Roy, N. C. M. Magdaong, H. Jing, J. Rong, J. R. Diers, H. S. Kang, D. M. Niedzwiedzki, M. Taniguchi, C. Kirmaier, J. S. Lindsey, D. F. Bocian and D. Holten, *J. Phys. Chem. A*, 2022, XXX, XXX–XXX. https://doi.org/10.1021/acs.jpca.2c06040.

61 J. R. Diers, C. Kirmaier, M. Taniguchi, J. S. Lindsey, D. F. Bocian and D. Holten, *Phys. Chem. Chem. Phys.,* 2021, **23**, 19130–19140.

62 M. Krayer, M. Ptaszek, H.-J. Kim, K. R. Meneely, D. Fan, K. Secor and J. S. Lindsey, *J. Org. Chem*., 2010, **75**, 1016–1039.

63 R. W. Wagner, T. E. Johnson, F. Li and J. S. Lindsey, *J. Org. Chem.,* 1995, **60**, 5266–5273.

64 R. W. Wagner, Y. Ciringh, C. Clausen and J. S. Lindsey, *Chem. Mater.,* 1999, **11**, 2974–2983.

65 D. Fan, M. Taniguchi and J. S. Lindsey, *J. Org. Chem.,* 2007, **72**, 5350–5357.

66 E. J. Alexy, J. M. Yuen, V. Chandrashaker, J. R. Diers, C. Kirmaier, D. F. Bocian, D. Holten and J. S. Lindsey, *Chem. Commun.,* 2014, **50**, 14512–14515.

67 M. Taniguchi, J. S. Lindsey, D. F. Bocian and D. Holten, *J. Photochem. Photobiol. C: Photochem. Rev.,* 2021, **46**, 100401.

68 N. C. M. Magdaong, H. Jing, J. R. Diers, C. Kirmaier, J. S. Lindsey, D. F. Bocian and D. Holten, *J. Phys. Chem. Lett.,* 2022, **13**, 7906–7910.

69 R. L. Martin, *J. Chem. Phys.,* 2003, **118**, 4775–4777.

70 J. Rong, N. C. M. Magdaong, M. Taniguchi, J. R. Diers, D. M. Niedzwiedzki, C. Kirmaier, J. S. Lindsey, D. F. Bocian and D. Holten, *J. Phys. Chem. A,* 2021, **125**, 7900–7919.

71 H. Jing, S. Liu, J. Jiang, V.-P. Tran, J. Rong, P. Wang and J. S. Lindsey, *New J. Chem.,* 2022, **46**, 5556–5572.

72 E. Yang, C. Kirmaier, M. Krayer, M. Taniguchi, H.-J. Kim, J. R. Diers, D. F. Bocian, J. S. Lindsey and D. Holten, *J. Phys. Chem. B,* 2011, **115**, 10801–10816.

73 E. Hindin, C. Kirmaier, J. R. Diers, K.-Y. Tomizaki, M. Taniguchi, J. S. Lindsey, D. F. Bocian and D. Holten, *J. Phys. Chem. B,* 2004, **108**, 8190–8200.

74 M. J. Frisch, G. W. Trucks, H. B. Schlegel, G. E. Scuseria, M. A. Robb, J. R. Cheeseman, G. Scalmani, V. Barone, B. Mennucci, G. A. Petersson, H. Nakatsuji, M. Caricato, X. Li, H. P. Hratchian, A. F. Izmaylov, J. Bloino, G. Zheng, J. L. Sonnenberg, M. Hada, M. Ehara, K. Toyota, R. Fukuda, J. Hasegawa, M. Ishida, T. Nakajima, Y. Honda, O. Kitao, H. Nakai, T. Vreven, J. A. Montgomery Jr., J. E. Peralta, F. Ogliaro, M. Bearpark, J. J. Heyd, E. Brothers, K. N. Kudin, V. N. Staroverov, R. Kobayashi, J. Normand, K. Raghavachari, A. Rendell, J. C. Burant, S. S. Iyengar, J. Tomasi, M. Cossi, N. Rega, J. M. Millam, M. Klene, J. E. Knox, J. B. Cross, V. Bakken, C. Adamo, J. Jaramillo, R. Gomperts, R. E. Stratmann, O. Yazyev, A. J. Austin, R. Cammi, C. Pomelli, J. W. Ochterski, R. L. Martin, K. Morokuma, V. G. Zakrzewski, G. A. Voth, P. Salvador, J. J. Dannenberg, S. Dapprich, A. D. Daniels, Ö. Farkas, J. B. Foresman, J. V. Ortiz, J. Cioslowski and D. J. Fox, Gaussian 09, version D.01, Gaussian, Inc., Wallingford CT, 2009.